Percolation Model of Sensory Transmission and Loss of Consciousness Under General Anesthesia

David W. Zhou,[1,5] David D. Mowrey,[1,2] Pei Tang,[1,2,3] and Yan Xu[1,3,4,*]

[1]*Department of Anesthesiology, University of Pittsburgh School of Medicine, Pittsburgh, Pennsylvania 15260, USA*
[2]*Department of Computational and Systems Biology, University of Pittsburgh School of Medicine, Pittsburgh, Pennsylvania 15260, USA*
[3]*Department of Pharmacology and Chemical Biology, University of Pittsburgh School of Medicine, Pittsburgh, Pennsylvania 15260, USA*
[4]*Department of Structural Biology, University of Pittsburgh School of Medicine, Pittsburgh, Pennsylvania 15260, USA*
[5]*Department of Biological Sciences, Carnegie Mellon University, Pittsburgh, Pennsylvania 15213, USA*

(Received 25 February 2015; published 4 September 2015)

Neurons communicate with each other dynamically; how such communications lead to consciousness remains unclear. Here, we present a theoretical model to understand the dynamic nature of sensory activity and information integration in a hierarchical network, in which edges are stochastically defined by a single parameter p representing the percolation probability of information transmission. We validate the model by comparing the transmitted and original signal distributions, and we show that a basic version of this model can reproduce key spectral features clinically observed in electroencephalographic recordings of transitions from conscious to unconscious brain activities during general anesthesia. As p decreases, a steep divergence of the transmitted signal from the original was observed, along with a loss of signal synchrony and a sharp increase in information entropy in a critical manner; this resembles the precipitous loss of consciousness during anesthesia. The model offers mechanistic insights into the emergence of information integration from a stochastic process, laying the foundation for understanding the origin of cognition.

DOI: 10.1103/PhysRevLett.115.108103 PACS numbers: 87.18.Sn, 87.18.Mp, 87.19.L–

Structural and functional neuroimaging studies have mapped the connectivity of neuroanatomy and networks at ever-increasing resolutions [1–5]. However, analyses that assign cognitive roles to structural or functional regions demonstrate a mechanism based on functionalism and not on neurobiological first principles, thus failing to bridge matter and mind [6]. In most analyses, cognition is claimed to arise in a large-scale functional network exhibiting coactivation of brain regions during a given task [4]. Although this definition of cognition usefully relates structure to function [4], its theoretical framework is circular and offers limited value in understanding the basic principles governing the emergence of cognition.

Circumventing this theoretical gap, several studies have modeled individual electroencephalographic (EEG) features associated with loss of consciousness during general anesthesia [7–15]. These include the use of dynamic causal modeling to describe EEG spectral power under anesthesia-induced unconsciousness [15], the use of metabolism dynamics to account for burst suppression [12], and the development of a stochastic model to describe general anesthesia as a thermodynamic phase transition [7,8]. In addition, a more detailed account of anesthetic effects on ion channels was used to parameterize a mean-field theory of electrocortical activities [16]. An information integration theory [17] treated consciousness as a unified state in a complex system that gains quantifiable information as a whole relative to the parts. An empirical measure was recently developed to assess information integration under different conscious states [18]. However, few theoretical advances explain multiple EEG features while accounting for information flow and integration *ab initio*, and without making causal assumptions of the system. A systems-level theory is needed to explain sensory processing under deep anesthesia [19]: No existing model accounts for EEG features under anesthesia, disruption of information flow, and neurobiological function together.

Here, we apply neurobiological first principles to information transmission in a neural network constructed on the basis of the thalamocortical and corticocortical topology. We use percolation theory [20] to calculate information access between nodes. By varying only one parameter governing the probability with which an edge is connected, the model reveals coherence emergence at a critical threshold. It generates stereotypical EEG features under general anesthesia while reproducing dose-response characteristics for loss of consciousness. Linking the loss and gain of information access to anesthesia induction and emergence, the model provides a fundamental theory of information emerging from a stochastic process and suggests that cognitive features are enabled as a phase transition.

We consider a layered hierarchical fractal structure ascending from an input node to multiple output nodes. The layered configuration abstracts laminar and divergent organization in mammalian thalamocortical structures [21–23] (see Fig. S1 in the Supplemental Material [24]). We create layers by scale-invariant fractal expansion and generate small-world properties among nodes within each

 © 2015 American Physical Society

layer using the Watts-Strogatz algorithm [27]. Scale invariance and small-world organization of brain networks have been well justified [28–33]. Edges are directional ($w_{ij} \neq w_{ji}$) to reflect the counterstream architecture of the human brain [34]. Importantly, we distinguish anterior from posterior nodes by assigning different edge weights in the feedforward and feedback directions.

Let $A_i(t)$ and $P_j(t)$ denote the neural activity of node i and the preceding input from node j at time t, respectively. $A_i(t)$ is the weighted average of activities from all input nodes,

$$A_i(t) = \frac{\sum_j w_{ij} P_j(t)}{\sum_j w_{ij}} = \frac{w_{ii} P_i(t) + \sum_{j \neq i} w_{ij} P_j(t)}{w_{ii} + \sum_{j \neq i} w_{ij}}, \quad (1)$$

where w_{ij} is the weight of a directional edge from node j to node i, and the input function $P_j(t)$ represents the accumulated history of neural activity from the preceding m time steps, weighted by exponentially decaying memory,

$$P_j(t) = \frac{\sum_{\tau=1}^{m} e^{-\tau} A_j(t-\tau)}{\sum_{\tau=1}^{m} e^{-\tau}}. \quad (2)$$

We used percolation theory [20] to stochastically assign weights w_{ij} to edges using a sampling function, with probability p representing likelihood of activity transmission,

$$w_{ij} = \begin{cases} \mathrm{CDF}(U[0,1]) & i \neq j \\ c e^{-\lambda \sum_{k \neq i} w_{ki}} & i = j \end{cases}, \quad (3)$$

where CDF is the Gaussian cumulative distribution function centered at $1 - p$ with a standard deviation of 0.05 (Fig. S2 [24]), $U[0, 1]$ is the standard uniform distribution, and c and λ are constants. As p is lowered, the probability of activity transmission along individual edges is reduced, representing the inhibition of information flow under anesthesia. Although different anesthetic classes act differently at molecular and cellular levels, with some potentiating inhibitory neurotransmission and others inhibiting excitatory neurotransmission, the net effect can be abstracted as a global inhibition of arousal [35]. For $i \neq j$, the sampling process of w_{ij} is independently varied by p. For $i = j$, w_{ii} is the memory of the past activity of the same node and is influenced by the incoming connection strength. Self-connection dominates when all non-self-connections diminish (i.e., when $\sum_{k \neq i} w_{ki} \to 0$). Because neuronal transmission, including axonal propagation and synaptic events, involves cycles of receptor inactivation, activation, and deactivation or desensitization, we account for this dynamic behavior by periodically resampling edge weights using the sampling process above. The resampling periodicity is proportional to $e^{-\alpha p}$, where α is a constant.

We first validate the theory against previous experimental EEG studies under general anesthesia, using several clinically observed features as evaluation criteria. Four key features are hallmarks of global EEG responses: (1) characteristic EEG waveforms, including burst suppression under deep anesthesia [36]; (2) an EEG power shift to lower frequencies with increasing anesthetic concentrations [37]; (3) synchronization of cortical nodes [38]; and (4) shift of α and δ power to the anterior, which is termed anteriorization [39]. Our model reproduces all of these clinical features simultaneously. The methods are detailed in the Supplemental Material [24].

Typical time-domain signals on a randomly selected output node are depicted in Fig. 1(a). Two different fractalizations yield a similar dependence on p. The waveforms strikingly resemble clinical EEG features under different anesthesia depths [40]. As p is lowered, the dominant output frequency decreases while the amplitude increases, as revealed by the spectral density in Fourier analyses [Fig. 1(b)]. Contrary to the simplistic picture of decreasing information flow during diminishing network connectivity, power rises significantly at $p = 0.7$ in the β

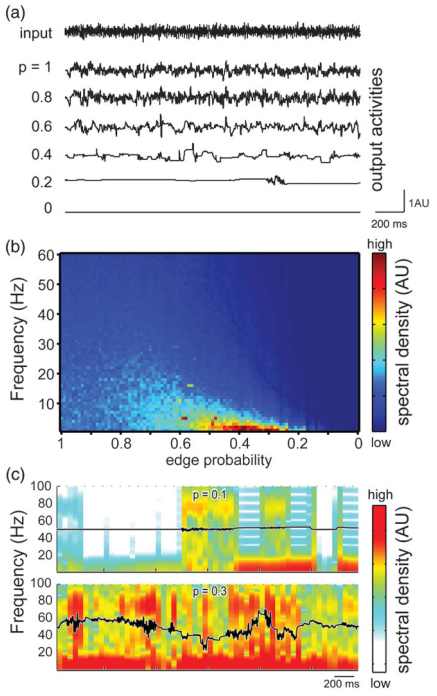

FIG. 1 (color). Information percolation in a neural network. (a) Output activities are plotted for various p on a randomly selected node in a one-to-four fractalization network. Input amplitude was scaled to $p = 1$. The output reproduces several clinical EEG features. At $p = 0.2$, burst suppression is observed. (b) Fourier analysis, averaged from 40 replicas on randomly selected output nodes, reveals a frequency shift upon network inhibition. Around $p = 0.7$, frequency shifts from the β to α range. Power concentrates toward the α and δ ranges with decreasing p. (c) Burst suppressions become evident at low p. Corresponding time-domain activities are superimposed onto spectrograms depicting frequency components of the bursts. Without losing generality, 50% random noises were added to a 115-Hz sinusoidal signal as input.

(12–30 Hz), α (8–12 Hz), θ (4–8 Hz), and δ (<4 Hz) ranges. When a critical portion of the edges is cut ($p \approx 0.5$–0.3), the spectral density rapidly concentrates into δ. At very low values of p, the network output exhibits bursting δ waves [Fig. 1(c)] that resemble burst suppression under deep anesthesia. As p approaches 0, the output flatlines, corresponding to isoelectric activity of a completely inhibited brain. These results agree with clinical observations of an EEG power shift from the γ and β bands to the α and δ bands during anesthesia [37].

The results from the model suggest that the underlying mechanism of burst suppression is edge resampling due to receptor desensitization and reactivation in a dynamic network. Decreasing p reduces the probability for signals to percolate to the cortex, leading to prolonged quiescence periods. However, when edge weights are dynamically refreshed, even at very low p, some signals transiently percolate through stochastically connected edges to reach the output layers, and appear as short bursts between long suppressions.

We also observe that frequency shift is an emergent phenomenon, occurring precipitously in a specific range of edge probabilities. The rapid power shift to lower frequencies matches clinical EEG features at a critical anesthetic concentration where consciousness is sharply and completely lost. Remarkably, this clinical feature is reproduced in random networks without a high graph density, suggesting that loss of consciousness is not localized to a specific set of neurons or receptor types, but is due to large-scale, distributed action on network connectivity. Importantly, this phenomenon is input invariant and intrinsic to the dynamic process of edge connectivity.

The synchronization of output with input occurs in the same frequency ranges when power concentrates to the β, α, and δ bands. Figure 2(a) displays input-posterior output synchronization; an identical pattern was observed between input and anterior output. When p is lowered to 0.5–0.7, cortical and thalamic nodes are strongly correlated in the β, α, and δ frequencies. As p is further lowered to 0.3–0.5, thalamocortical coupling exhibits a narrow band of strong synchronization in the γ (30–75 Hz) and β (16–30 Hz) bands. The appearance of this strong thalamocortical synchrony at $p \sim 0.3$ indicates information integration, whereby chaotic signals at $p < 0.3$ become ordered and recognizable in the output. The γ activity in a severely inhibited network is similar to near-death EEG activity [41]. Corticocortical synchronization was also observed among output nodes. Agreeing with clinical observations under deep anesthesia [38,42,43], corticocortical synchronization in a heavily cut network occurs predominantly in the δ and θ frequency ranges [Fig. 2(b)].

EEG anteriorization during anesthesia reflects asymmetric network activity. To understand its underlying mechanism, we investigated various conditions that could support asymmetric distribution of spectral power when p was

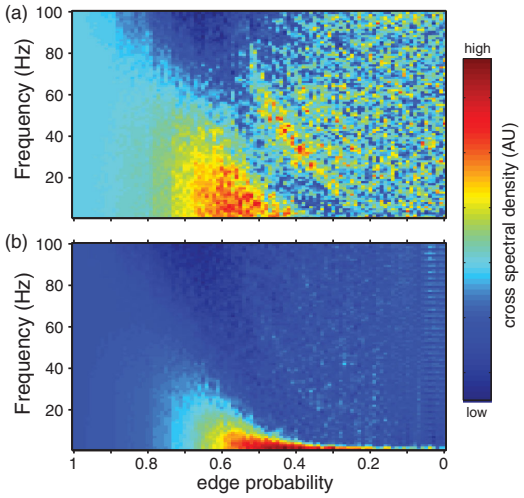

FIG. 2 (color). Thalamocortical and corticocortical coherence. (a) Thalamocortical coherence, measured as cross-spectral density averaged from 40 replicas on randomly selected posterior nodes, is plotted as a function of p. Patterns for anterior nodes are similar. Until $p \approx 0.8$, no coherent activity is dominant at any frequency. With further inhibition, thalamocortical coherence appears in the β range, and it lowers to the α range at $p \approx 0.6$. Between $p \approx 0.5$–0.3, a band of γ coherence is visible. (b) Corticocortical coherence between two randomly selected nodes in the output layer appears in the α and δ ranges for $p < 0.6$. Coherence frequencies further decrease with p. To maximize test stringency, simulations were performed using random noise as input.

reduced. We observed anteriorization only when feedback weights were greater than feedforward weights. Figure 3 displays Fourier transformations of neural activity in the outermost layer of a four-degree five-layer fractal network. Anteriorization is evident in the α and δ frequencies when the feedback:feedforward ratio is 10:1, and it co-occurs with frequency downshift and thalamocortical synchronization, signifying a shared mechanism of the same statistical process. Altering ascending projection probabilities to anterior or posterior nodes failed to produce anteriorization, which suggests that anteriorization results from the inhibition of corticocortical rather than thalamocortical communications. Literature on the comparative density of feedback projections in the visual system supports this finding [3,34,44,45]. Although counterintuitive, the result underscores fundamental differences between steady-state and dynamic networks, in which the response to change dominates the output. As edges are incrementally cut, a network with denser (greater weight) feedback projections has a disproportionally higher probability of losing its feedback information flow. Our model suggests that shifts of low-frequency power to the network anterior result from an exaggerated disruption in the feedback direction. This offers an alternative interpretation for the preferential inhibition of feedback connectivity during general anesthesia [46], which occurs due to a higher baseline density of feedback connectivity under unanesthetized conditions.

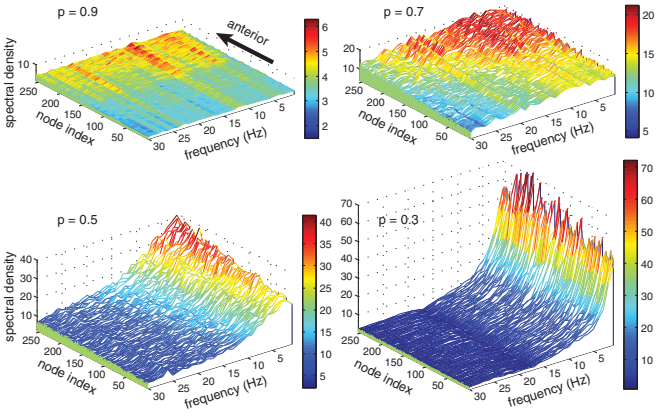

FIG. 3 (color). Anteriorization of cortical activity. Fourier analyses of output node activity for the indicated edge probabilities are shown. Output nodes are arranged 1 to 256 in groups of 16 from posterior to anterior. Higher power in the α and δ bands shifts to the anterior (higher number) nodes with decreasing p until $p = 0.3$, when anteriorization effects dissipate.

Our model makes no *a priori* assumptions about molecular, cellular, or metabolic mechanisms of the network, nor does it specify constraints on connections within layers; this ensures the system's universality and scalability. By conceptualizing global arousal as stochastic edge percolation among brain centers, our model is necessarily coarse-grained; it does not consider drug- and receptor-specific properties. Yet the success of such a simple statistical model in producing multiple salient EEG features under anesthesia suggests that it simulates information transmission at a fundamental level and provides theoretical confidence in its predictive power.

A theoretical prediction, which is of general interest in neuroscience, is when and how cognitive features, such as sensory access, arise in an artificial network. We use the criticality of a chaos-order state transition as a surrogate measure to define the accessibility of information-encoding dynamics of a given node at other nodes. We determined conditions under which information is statistically preserved by analyzing the divergence of the time-domain signal distributions when the output at a randomly selected node is used to represent the input. We quantified percolation loss as an increase in bitwise information entropy measured by Kullback-Leibler (KL) divergence, or $\mathrm{KL}(P\|Q)$, where P and Q are probability distributions of input and output, respectively [47]. An order parameter is defined, as detailed in the Supplemental Material [24]. Figure 4 shows how order emerges sharply as the network's edge probability increases from 0 to 1. Information entropy [Fig. 4(a)] drops precipitously at $p \approx 0.3$. The dichotomous dependence of KL divergence on p for encoded information content is plotted in Fig. 4(b). A clear phase transition—with more pronounced fluctuations—occurs around $p \approx 0.3$. To illustrate this transition graphically, we percolated a time series encoding the pixel intensities of an 8-bit grayscale image through the network under different values of p, and examined the threshold at which the integrity of the image was "recognizable" in the output layer. We calculated $\mathrm{KL}(P\|Q) - \mathrm{KL}_c$ for 256 different intensities (8 bits of information) with systematically varied values of p. Each output pixel intensity was determined stochastically from $2^{[\mathrm{KL}(P\|Q)-\mathrm{KL}_c]}$ random values between 0 and 256 (i.e., $\mathrm{KL}(P\|Q) - \mathrm{KL}_c$ bits of information) including the correct pixel intensity in the input image. Figure 4(c) shows a series of images decoded randomly at any node in the output layer at different percolation probabilities. A discernible image emerges sharply between $p = 0.30$ and $p = 0.32$. Recall that thalamocortical synchronization emerges in the γ and β band in the same range of p [Fig. 2(a)].

The sharp emergence of order with a precipitous drop in entropy approximates the steep dose-response curve for transitions between brain states during general anesthesia. More remarkably, no network connection is deterministic, because weight reassignments stochastically switch any given edge between open and closed. Moreover, graph density in our network is relatively sparse, suggesting that supporting high-level information features does not require dense connectivity. That the integrity of the input image in Fig. 4 is partially maintained and recognizable at $p \approx 0.3$ suggests a low information-emergence threshold. Indeed, the probability for information percolating from input to any output node at $p \approx 0.3$ is <0.0081 for the shortest path, yet inhibition at this level is robustly tolerated. The underlying process for burst suppressions, discussed above, likely contributes to the network's ability to integrate information at low p. This implies that information access can occur in simple systems as long as some type of pacemaking activity exists to coordinate the dynamic recalibration of connection strength among the network components. In mammalian brains, pacemakers are known to exist [48–50] and their neurobiological description is consistent with this notion.

Our model has been built to provide a global view of rules governing information percolations through scalable brain connectivity, without considering many biological details. For example, we do not differentiate network inhibition through potentiation of inhibitory neurons or inhibition of excitatory neurons. Similarly, regional heterogeneities due to different populations of receptor subtypes are not considered. Although adding more realism will likely provide more quantitative power to explain specific experimental observations, these details will not invalidate the general conclusions on the global scale, as evidenced by the model's qualitative robustness in reproducing clinical EEG features with only a single parameter.

This model has important theoretical implications and supports the notion that consciousness may arise from the same basic statistical processes as those governing the criticality for self-organization emergence, independent of biological details [51]. Although the brain is many orders of magnitude more complex, it is tempting to speculate that the

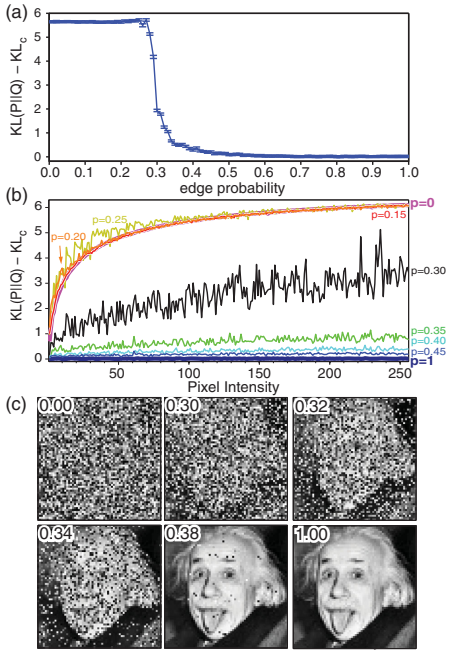

FIG. 4 (color). Emergence of correlative signal cohesion. (a) Output information entropy, measured by the KL divergence $[\mathrm{KL}(P\|Q) - \mathrm{KL}_c]$ as an order parameter, is plotted as a function of p. Each value represents bits lost in the output from 8 bits of maximum information. A phase transition is revealed at $p \approx 0.3$. (b) KL divergence plotted as a function of pixel intensity for $p = 0$ (purple), 0.15 (red), 0.20 (orange), 0.25 (yellow), 0.30 (black), 0.35 (green), 0.40 (cyan), 0.45 (blue), and 1 (dark blue). Similar to (a), a clear dichotomy in information entropy occurs around $p = 0.3$. Information content is lost more rapidly from high-intensity signals. (c) Graphic illustration of transitions revealed in (a) and (b): Reconstructions of an 8-bit gray scale image at $p = 0.00$, 0.30, 0.32, 0.34, 0.38, and 1.00, respectively. The original image features emerge sharply, becoming recognizable between $p = 0.32$ and $p = 0.34$.

transition between conscious and unconscious states is also regulated by a single connectivity parameter, especially considering the clinical observation that a sharp transition between conscious and unconscious states occurs within an extremely narrow anesthetic concentration range, with little variation among human subjects or even among different species of vastly different brain scales and capacities.

Experimentalists may test this model by measuring organized synchronous activity in brain networks, such as between the primary visual cortex and frontal eye fields. A critical anesthetic dose might be identified where synchronous firing for visual attention is abruptly disrupted upon loss of consciousness. It is also possible to design a double transgenic system [52] with two reporters driven by activity-dependent immediate early genes. A comparison of the colocalization of the reporters should reveal a fixed subset of neurons in conscious learning and relearning, but an increasingly chaotic, nonoverlapping subset of neurons in unconscious learning under varying anesthesia depths. Our model also raises the possibility of statistically improbable brain states, in which deeply inhibited neural centers become sufficiently connected through stochastic processes to a degree that they can support consciousness markers. Clinically, this may suggest the possibility of information incorporation in minimally conscious brains. Recent experiments in rodents have demonstrated such possibilities [19].

This work was supported by grants from the National Institutes of Health (Grants No. R37GM049202 and No. R01GM066358) and the IEEE Computational Intelligence Society. D. W. Z. and D. D. M. contributed equally to this work.

*Corresponding author.
xuy@anes.upmc.edu

[1] R. D. S. Raizada, Towards a theory of the laminar architecture of cerebral cortex: computational clues from the visual system, Cereb. Cortex **13**, 100 (2003).
[2] J. A. Hirsch and L. M. Martinez, Laminar processing in the visual cortical column, Curr. Opin. Neurobiol. **16**, 377 (2006).
[3] N. T. Markov *et al.*, A weighted and directed interareal connectivity matrix for macaque cerebral cortex, Cereb. Cortex **24**, 17 (2014).
[4] S. L. Bressler and V. Menon, Large-scale brain networks in cognition: emerging methods and principles, Trends Cognit. Sci. **14**, 277 (2010).
[5] V. Menon, Large-scale brain networks and psychopathology: a unifying triple network model, Trends Cognit. Sci. **15**, 483 (2011).
[6] H. J. Park and K. Friston, Structural and functional brain networks: from connections to cognition, Science **342**, 1238411 (2013).
[7] M. L. Steyn-Ross, D. A. Steyn-Ross, J. W. Sleigh, and L. C. Wilcocks, Toward a theory of the general-anesthetic-induced phase transition of the cerebral cortex. I. A thermodynamics analogy, Phys. Rev. E **64**, 011917 (2001).
[8] D. A. Steyn-Ross, M. L. Steyn-Ross, L. C. Wilcocks, and J. W. Sleigh, Toward a theory of the general-anesthetic-induced phase transition of the cerebral cortex. II. Numerical simulations, spectral entropy, and correlation times, Phys. Rev. E **64**, 011918 (2001).
[9] M. L. Steyn-Ross, D. A. Steyn-Ross, J. W. Sleigh, and D. T. Liley, Theoretical electroencephalogram stationary spectrum for a white-noise-driven cortex: evidence for a general anesthetic-induced phase transition, Phys. Rev. E **60**, 7299 (1999).
[10] K. Wang, M. L. Steyn-Ross, D. A. Steyn-Ross, M. T. Wilson, and J. W. Sleigh, EEG slow-wave coherence changes in propofol-induced general anesthesia: experiment and theory, Front. Syst. Neurosci. **8**, 215 (2014).
[11] S. N. Ching, A. Cimenser, P. L. Purdon, E. N. Brown, and N. J. Kopell, Thalamocortical model for a propofol-induced α-rhythm associated with loss of consciousness, Proc. Natl. Acad. Sci. U.S.A. **107**, 22665 (2010).
[12] S. N. Ching, P. L. Purdon, S. Vijayan, N. J. Kopell, and E. N. Brown, A neurophysiological—metabolic model for burst suppression, Proc. Natl. Acad. Sci. U.S.A. **109**, 3095 (2012).

[13] T. Iwai, H. Kihara, K. Imaiand, and M. Uchida, Dose-response curve for anaesthetics based on the Monod-Wyman-Changeux model, Br. J. Anaesth. **77**, 517 (1996).
[14] J. H. Sheeba, A. Stefanovska, and P. V. E. McClintock, Neuronal synchrony during anaesthesia - A thalamocortical model, Biophys. J. **95**, 2722 (2008).
[15] M. M. Boly *et al.*, Connectivity changes underlying spectral EEG changes during propofol-induced loss of consciousness, J. Neurosci. **32**, 7082 (2012).
[16] I. Bojak and D. T. Liley, Modeling the effects of anesthesia on the electroencephalogram, Phys. Rev. E **71**, 041902 (2005).
[17] G. Tononi, Consciousness as integrated information: a provisional manifesto, Biol. Bull. **215**, 216 (2008).
[18] A. G. Casali *et al.*, A theoretically based index of consciousness independent of sensory processing and behavior, Sci. Transl. Med. **5**, 198ra105 (2013).
[19] A. R. Samuelsson, N. R. Brandon, P. Tang, and Y. Xu, Cellular registration without behavioral recall of olfactory sensory input under general anesthesia, Anesthesiology **120**, 890 (2014).
[20] B. Bollobas and O. Riordan, *Percolation* (Cambridge University Press, Cambridge, England, 2006).
[21] S. M. Sherman, Thalamocortical interactions, Curr. Opin. Neurobiol. **22**, 575 (2012).
[22] N. Yamamoto, Cellular and molecular basis for the formation of lamina-specific thalamocortical projections, Neurosci. Res. **42**, 167 (2002).
[23] M. Inan and M. C. Crair, Development of cortical maps: perspectives from the barrel cortex, Neuroscientist **13**, 49 (2007).
[24] See Supplemental Material at http://link.aps.org/supplemental/10.1103/PhysRevLett.115.108103, which includes Refs. [25,26].
[25] T. Fedele, H. J. Scheer, G. Waterstraat, B. Telenczuk, M. Burghoff, and G. Curio, Towards non-invasive multi-unit spike recordings: mapping 1 kHz EEG signals over human somatosensory cortex, Clin. Neurophysiol. **123**, 2370 (2012).
[26] H. J. Scheer, T. Fedele, G. Curio, and M. Burghoff, Extension of non-invasive EEG into the kHz range for evoked thalamocortical activity by means of very low noise amplifiers, Physiol. Meas. **32**, N73 (2011).
[27] D. J. Watts and S. H. Strogatz, Collective dynamics of 'small-world' networks, Nature (London) **393**, 440 (1998).
[28] F. Aboitiz and J. F. Montiel, From tetrapods to primates: conserved developmental mechanisms in diverging ecological adaptations, Prog. Brain Res. **195**, 3 (2012).
[29] N. Kadmon Harpaz, T. Flash, and I. Dinstein, Scale-invariant movement encoding in the human motor system, Neuron **81**, 452 (2014).
[30] G. Werner, Fractals in the nervous system: conceptual implications for theoretical neuroscience, Front. Physiol. **1**, 15 (2010).
[31] C. T. Kello, G. D. Brown, I. C. R. Ferrer, J. G. Holden, K. Linkenkaer-Hansen, T. Rhodes, and G. C. Van Orden, Scaling laws in cognitive sciences, Trends Cognit. Sci. **14**, 223 (2010).
[32] C. J. Stam and E. C. van Straaten, The organization of physiological brain networks, Clin. Neurophysiol. **123**, 1067 (2012).
[33] O. Sporns, D. R. Chialvo, M. Kaiser, and C. C. Hilgetag, Organization, development and function of complex brain networks, Trends Cognit. Sci. **8**, 418 (2004).
[34] N. T. Markov, M. Ercsey-Ravasz, D. C. Van Essen, K. Knoblauch, Z. Toroczkai, and H. Kennedy, Kennedy, Cortical high-density counterstream architectures, Science **342**, 1238406 (2013).
[35] E. N. Brown, P. L. Purdon, and C. J. Van Dort, General anesthesia and altered states of arousal: a systems neuroscience analysis, Annu. Rev. Neurosci. **34**, 601 (2011).
[36] K. M. Hartikainen, M. Rorarius, J. J. Peräkylä, P. J. Laippala, and V. Jäntti, Cortical reactivity during isoflurane burst-suppression anesthesia, Anesth. Analg. **81**, 1223 (1995).
[37] V. A. Feshchenko, R. A. Veselis, and R. A. Reinsel, Propofol-induced alpha rhythm, Neuropsychobiology **50**, 257 (2004).
[38] G. G. Supp, M. Siegel, J. F. Hipp, and A. K. Engel, Cortical hypersynchrony predicts breakdown of sensory processing during loss of consciousness, Curr. Biol. **21**, 1988 (2011).
[39] J. H. Tinker, F. W. Sharbrough, and J. D. Michenfelder, Anterior shift of the dominant EEG rhytham during anesthesia in the Java monkey: Correlation with anesthetic potency, Anesthesiology **46**, 252 (1977).
[40] D. L. Clark and B. S. Rosner, Neurophysiologic effects of general anesthetics. I. The electroencephalogram and sensory evoked responses in man, Anesthesiology **38**, 564 (1973).
[41] J. Borjigin, U. Lee, T. Liu, D. Pal, S. Huff, D. Klarr, J. Sloboda, J. Hernandez, M. M. Wang, and G. A. Mashour, Surge of neurophysiological coherence and connectivity in the dying brain, Proc. Natl. Acad. Sci. U.S.A. **110**, 14432 (2013).
[42] M. Steriade, D. Contreras, F. Amzica, and I. Timofeev, Synchronization of fast (30–40 Hz) spontaneous oscillations in intrathalamic and thalamocortical networks, J. Neurosci. **16**, 2788 (1996).
[43] D. Contreras and M. Steriade, Synchronization of low-frequency rhythms in corticothalamic networks, Neuroscience (N.Y.) **76**, 11 (1996).
[44] J. Vezoli, A. Falchier, B. Jouve, K. Knoblauch, M. Young, and H. Kennedy, Quantitative analysis of connectivity in the visual cortex: extracting function from structure, Neuroscientist **10**, 476 (2004).
[45] D. J. Felleman and D. C. Van Essen, Distributed hierarchical processing in the primate cerebral cortex, Cereb. Cortex **1**, 1 (1991).
[46] U. Lee, S. Kim, G. J. Noh, B. M. Choi, E. Hwang, and G. A. Mashour, The directionality and functional organization of frontoparietal connectivity during consciousness and anesthesia in humans, Conscious. Cogn. **18**, 1069 (2009).
[47] S. Kullback and R. A. Leibler, On Information and Sufficiency, Ann. Math. Stat. **22**, 79 (1951).
[48] P. Fuentealba and M. Steriade, The reticular nucleus revisited: intrinsic and network properties of a thalamic pacemaker, Prog. Neurobiol. **75**, 125 (2005).
[49] J. R. Huguenard, Anatomical and physiological considerations in thalamic rhythm generation, J. Sleep Res. **7**, 24 (1998).
[50] D. Jaeger and H. Kita, Functional connectivity and integrative properties of globus pallidus neurons, Neuroscience (N.Y.) **198**, 44 (2011).
[51] D. Krotov, J. O. Dubuis, T. Gregor, and W. Bialek, Morphogenesis at criticality, Proc. Natl. Acad. Sci. U.S.A. **111**, 3683 (2014).
[52] N. Matsuo, Irreplaceability of neuronal ensembles after memory allocation, Cell Rep. **11**, 351 (2015).